

# Economical Jet Taggers - Equivariant, Slim, and Quantized

Antoine Petitjean<sup>1</sup>, Tilman Plehn<sup>1,2</sup>, Jonas Spinner<sup>3</sup>, and Ullrich Köthe<sup>2</sup>

**1** Institut für Theoretische Physik, Universität Heidelberg, Germany

**2** Interdisciplinary Center for Scientific Computing (IWR), Universität Heidelberg, Germany

**3** Institute for Particle Physics Phenomenology, Durham University, UK

December 22, 2025

## Abstract

Modern machine learning is transforming jet tagging at the LHC, but the leading transformer architectures are large, not particularly fast, and training-intensive. We present a slim version of the L-GATr tagger, reduce the number of parameters of jet-tagging transformers, and quantize them. We compare different quantization methods for standard and Lorentz-equivariant transformers and estimate their gains in resource efficiency. We find a six-fold reduction in energy cost for an moderate performance decrease, down to 1000-parameter taggers. This might be a step towards trigger-level jet tagging with small and quantized versions of the leading equivariant transformer architectures.

---

## Contents

<b>1</b> Introduction	<b>2</b>
<b>2</b> L-GATr-slim	<b>3</b>
2.1 Lorentz-scalars and vectors	3
2.2 Jet tagging	4
2.3 Amplitude regression	6
2.4 Event generation	7
2.5 Ultra-mini taggers	8
<b>3</b> Quantized jet taggers	<b>9</b>
3.1 Low-precision data types	9
3.2 Weight quantization	10
3.3 Quantized equivariant taggers	12
3.4 Towards online jet tagging	14
<b>4</b> Outlook	<b>15</b>
<b>A</b> Implementation details	<b>16</b>
<b>References</b>	<b>17</b>

---

## 1 Introduction

Modern machine learning (ML) is reshaping the research program at the LHC. Even for standard analyses, triggering, data acquisition, object identification, first-principle simulations, and optimal inference are changing rapidly [1]. Among the most established ML applications in LHC physics are jet taggers [2, 3]. Their goal is to utilize the complete information about the jet substructure to determine their partonic nature [4–9]. This question leads directly to the input and latent data representations, from image-inspired architectures to graphs and transformers for a permutation-invariant point cloud. In addition, jet taggers were shown to benefit from the fundamental Lorentz symmetry [10]. This motivated a series of Lorentz-equivariant graph-networks taggers [11–15], where in physics we would use the term ‘covariant’ rather than ‘equivariant’. The final step of the development of equivariant taggers is marked by Lorentz-equivariant transformers with learned symmetry breaking, using either a geometric algebra representation [16] or symmetry-linked local reference frames for each constituent [17]. Their advantage over the corresponding graph networks is that transformers benefit significantly more from larger training datasets.

An alternative path to high-performance taggers is pre-training of larger and larger transformers, with the implicit assumption that they learn the underlying physics structures [16–20]. Upscaling networks and training datasets is inspired by industry applications and has become the standard method to roll out increasingly powerful ML-tools. However, in LHC physics we have to account for many limiting factors, which can include the memory usage of the standard analysis hardware or specific hardware used for event triggering. For triggering, jet classification does not yet play a role, but it definitely should [21–24]. This leads us to asking the inverse question: *How small and how efficient can we make modern jet taggers with limited performance loss?*.

The first and immediate question is how small and how fast we can make an equivariant transformer, assuming that symmetry-aware data representations will improve training and performance under constraints. In Sec. 2, we present and benchmark a streamlined version of L-GATr that uses a more efficient latent representation based only on scalars and vectors. From a representation learning perspective, the slim Lorentz-equivariant tagger can be applied to many LHC tasks, from jet tagging to amplitude regression and event generation. In Sec. 2.5 we compare the performance of L-GATr-slim and LLoCa taggers [17] down to 1000-parameter networks, either with a reduced number of layers or with a reduced numbers of parameters per layer.

The comparison between the L-GATr-slim and LLoCa taggers provides us with a baseline for further computational optimization in Sec. 3. In this second step we quantize the equivariant taggers. Optimized parameter types are an established strategy for large language models, using different precision for different network layers to reduce computational cost and energy consumption. In Sec. 3.2 we introduce weight quantization of the linear layers via a regularization constraint implemented with the proximal gradient method, leading to piecewise-affine regularized quantization (PARQ), and straight-through estimation (STE) as a special case. We apply this quantization to Lorentz-equivariant taggers in Sec. 3.3. We find that they can be quantized like standard networks, leading to a significant efficiency gain with minimal performance loss. Finally, in Sec. 3.4 we combine both strategies to develop truly minimal, i.e. small and quantized versions of the leading tagger architectures. Such maximally resource-efficient versions might become useful for triggering at the HL-LHC.

## 2 L-GATr-slim

The standard data representation for neural networks applied to LHC physics is point clouds, including 4-vectors for each particle, jet constituent, or partons. The two symmetries governing these 4-vectors are permutations and Lorentz transformations. Graph-based and transformer architectures ensure permutation invariance. Explicit Lorentz equivariance with learned symmetry breaking in the network architecture has been shown to lead to significant performance improvements for graph networks [11–15] and for transformers [16, 17]. The key advantage of transformers over other graph network architectures is their superior scaling: they train efficiently on large datasets thanks to highly parallelizable attention, often yielding the best performance as data and model size grow.

There exist two fundamentally different implementations of Lorentz-equivariant transformers. First, L-GATr [16] expresses input and output using a geometric algebra representation and replaces the transformer layers with operations that keep track of scalar, pseudo-scalar, vector, axial-vector, and antisymmetric rank-two tensor components. Second, LLoCa [17] assigns a local reference frame to each 4-vector, represents latent features as invariants in these frames, and incorporates Lorentz transformations into the message passing. Both architectures give comparable performance on standard LHC tasks, such as amplitude regression, top tagging, and event generation. As the pseudo-scalar, axial-vectors, and tensor representations in L-GATr are not needed for most LHC applications [14], we develop a slim L-GATr architecture that only uses scalars and vectors.

### 2.1 Lorentz-scalars and vectors

The L-GATr-slim architecture generalizes standard transformer building blocks to operate on coupled scalar  $s$  and vector  $v$  representations:

- First, we extend the scalar linear layer by a linear operation acting on vectors, where all vector components are multiplied by the same learnable scalar coefficient. Different scalar coefficients for the vector components would violate Lorentz equivariance. This operation is equivalent to the L-GATr linear layer,

$$\text{Linear}(x) = \text{Linear} \begin{pmatrix} s \\ v \end{pmatrix} = \begin{pmatrix} \text{Linear}_s(s) \\ \text{Linear}_v(v) \end{pmatrix} = \begin{pmatrix} w_s \cdot s + b_s \\ w_v \cdot v \end{pmatrix} \quad (1)$$

with  $s \in \mathbb{R}^{c_s^{\text{in}}}$   $w_s \in \mathbb{R}^{c_s^{\text{out}} \times c_s^{\text{in}}}$   $b_s \in \mathbb{R}^{c_s^{\text{out}}}$   $v \in \mathbb{R}^{c_v^{\text{in}} \times 4}$   $w_v \in \mathbb{R}^{c_v^{\text{out}} \times c_v^{\text{in}}}$ .

- For the nonlinearity we extend the Gated Linear Unit (GLU) [25]. Instead of directly applying the GELU nonlinearity to the linear layer output, GLU multiplies these activations with the output of a second linear layer. We adapt this idea to the vector channel by applying the nonlinearity to the inner product of two vectors, and multiply it by the vector output of the L-GATr-slim linear layer,

$$\text{GLU} \begin{pmatrix} s \\ v \end{pmatrix} = \begin{pmatrix} \text{GELU}(\text{Linear}_{s,1}(s)) \text{Linear}_{s,2}(s) \\ \text{GELU}(\langle \text{Linear}_{v,1}(v), \text{Linear}_{v,2}(v) \rangle) \text{Linear}_{v,3}(v) \end{pmatrix}. \quad (2)$$

$\text{Linear}_{s,j}$  and  $\text{Linear}_{v,j}$  denote different linear layers, but implemented as one fused linear operation with an increased output dimensionality, by a factor two for scalars and a factor three for vectors. When using GLU we follow the common practice of increasing the number of output channels by another factor of two compared to the number of input channels.

- Next, we modify the standard RMSNorm to account for the geometric properties of vector channels. We use the absolute value of the Minkowski inner product to evaluate the vector

contribution to the norm. The absolute value is required, because the Minkowski inner product can become negative. This is very similar to L-GATr, with the only difference that L-GATr normalizes multivectors and scalars separately,

$$\text{RMSNorm} \begin{pmatrix} s \\ v \end{pmatrix} = \left( \frac{1}{c_v} \sum_{c=1}^{c_v} |\langle v_c, v_c \rangle|^2 + \frac{1}{c_v} \sum_{c=1}^{c_v} s_c^2 + \epsilon \right)^{-1/2} \begin{pmatrix} s \\ v \end{pmatrix}. \quad (3)$$

- Finally, we construct the scalar attention closely following L-GATr,

$$\text{Attention} \begin{pmatrix} q_s, k_s, v_s \\ q_v, k_v, v_v \end{pmatrix}_i = \sum_{j=1}^{n_t} \text{Softmax}_j \left( \frac{\sum_{c=1}^{c_s} q_{s,ic} k_{s,jc} + \sum_{c=1}^{c_v} \langle q_{v,ic}, k_{v,jc} \rangle}{\sqrt{4n_v + n_s}} \right) \begin{pmatrix} v_s \\ v_v \end{pmatrix}_j. \quad (4)$$

The inner product is implemented as a list of prefactors multiplied onto the query vector before evaluating the (euclidean) inner product using optimized attention kernels. The token dimensionality is  $n_t$ .

We combine these layers into the L-GATr-slim transformer architecture,

$$\begin{aligned} \bar{x} &= \text{RMSNorm}(x) \\ \text{AttentionBlock}(x) &= \text{Linear} \circ \text{Attention}(\text{Linear}(\bar{x}), \text{Linear}(\bar{x}), \text{Linear}(\bar{x})) + x \\ \text{MLPBlock}(x) &= \text{Linear} \circ \text{GLU}(\bar{x}) + x \\ \text{Block}(x) &= \text{MLPBlock} \circ \text{AttentionBlock}(x) \\ \text{L-GATr-slim}(x) &= \text{Linear} \circ \text{Block} \circ \text{Block} \circ \dots \circ \text{Block} \circ \text{Linear}(x) \end{aligned} \quad (5)$$

The main difference to L-GATr is the reduced number of hidden components/channels and the fact that our L-GATr-slim implementation can be compiled with `torch.compile` to increase computing efficiency. Moreover, L-GATr-slim uses slightly different designs for the normalization and nonlinearity that simplify the processing of scalars and vectors through the network without sacrificing performance. We find that it matches the L-GATr performance even without an outer product, so we drop this operation to save significant extra computational cost.

## 2.2 Jet tagging

Because our focus will be jet tagging, we first show the L-GATr-slim performance for the standard top tagging benchmark [2]. We compare our slim architecture to other leading architectures in Tab. 1 and find that it matches the performance of L-GATr, the LLoCa-Transformer, and different Lorentz-equivariant graph networks. The hyperparameters for the full-sized L-GATr-slim are given in App. A. For details on the established networks and their hyperparameters we refer to Ref. [17]. Because detector effects violate Lorentz symmetry, the tagger has to be able to incorporate the corresponding symmetry breaking. To allow for that, we keep the beam and time axes as an additional input particles.

Next, we benchmark L-GATr-slim on the larger JetClass dataset, covering light quark or gluon jets,  $Z$ ,  $W$ , and  $H$  jets, as well as top jets. The dataset contains 10M training jets for each of the ten different jet labels. The performance metric is the AUC averaged over all pairs of classes. Again, L-GATr-slim reproduces the performance of other leading Lorentz-equivariant transformers. In addition, L-GATr-slim has the same computational cost as the LLoCa-Transformer and is significantly more efficient than L-GATr, in terms of FLOPs, memory consumption, and training time.

The developments of modern jet taggers from the classic 2017 BDT is illustrated in the left panel of Fig. 1. We note that the highest-performing taggers, denoted as f.t. for fine-tuned, are

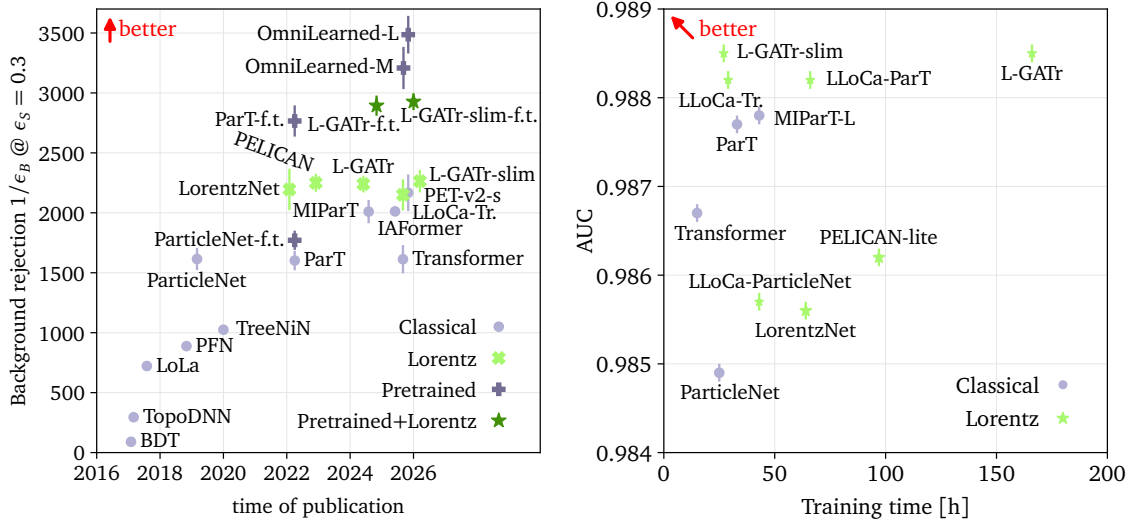


Figure 1: Left: Progress in top tagging through advanced network architectures over time. Right: Efficiency of tagging architectures on the JetClass dataset.

pretrained on increasingly large datasets, as can be seen in Tab. 1. In the right panel of Fig. 1 we show the same taggers, measuring the performance in AUC for a given training time on a single H100 GPU. This shows that performance is not automatically correlated with computing cost and motivates the development of resource-efficient networks for LHC analyses.

Network	Accuracy	AUC	$1/\epsilon_B$ ( $\epsilon_S = 0.5$ )	$1/\epsilon_B$ ( $\epsilon_S = 0.3$ )	# Params	# Train
ParticleNet [9]	0.940	0.9858	$397 \pm 7$	$1615 \pm 93$	0.4M	1.2M
Transformer [17]	0.9393	$0.9855 \pm 0.0001$	$389 \pm 6$	$1613 \pm 118$	2.0M	1.2M
ParT [18]	0.940	0.9858	$413 \pm 16$	$1602 \pm 81$	2.1M	1.2M
MIParT [26]	0.942	0.9868	$505 \pm 8$	$2010 \pm 97$	2.2M	1.2M
IAFormer [27]	0.942	0.987	$510 \pm 6$	$2012 \pm 30$	0.2M	1.2M
PET v2-s [19]	0.943	0.987	$505 \pm 14$	$2167 \pm 153$	3.0M	1.2M
LorentzNet* [11]	0.942	0.9868	$498 \pm 18$	$2195 \pm 173$	0.2M	1.2M
PELICAN* [28]	0.9426	$0.9870 \pm 0.0001$	–	$2250 \pm 75$	0.2M	1.2M
CGENN* [15]	0.942	0.9869	500	2172	0.3M	1.2M
LLoCa-Transformer* [17]	0.9416	$0.9866 \pm 0.0001$	$492 \pm 15$	$2150 \pm 130$	2.0M	1.2M
L-GATr* [16]	0.9423	$0.9870 \pm 0.0001$	$540 \pm 20$	$2240 \pm 70$	1.1M	1.2M
L-GATr-slim*	0.9420	$0.9869 \pm 0.0001$	$546 \pm 7$	$2264 \pm 93$	2.0M	1.2M
ParticleNet-f.t. [18]	0.942	0.9866	$487 \pm 9$	$1771 \pm 80$	0.4M	100M
OmniLearn [29]	0.942	0.9872	$568 \pm 9$	$2647 \pm 192$	2.0M	100M
ParT-f.t. [18]	0.944	0.9877	$691 \pm 15$	$2766 \pm 130$	2.1M	100M
MIParT-f.t. [26]	0.944	0.9878	$640 \pm 10$	$2789 \pm 133$	2.3M	100M
L-GATr-f.t.* [16]	0.9446	0.9879	$651 \pm 11$	$2894 \pm 84$	1.1M	100M
L-GATr-slim-f.t.*	0.9442	0.9879	$655 \pm 5$	$2927 \pm 70$	2.0M	100M
OmniLearned-M [19]	0.944	0.9880	$656 \pm 12$	$3208 \pm 176$	58M	1058M
OmniLearned-L [19]	0.944	0.9880	$688 \pm 9$	$3486 \pm 157$	423M	1058M

Table 1: Top tagging accuracy, AUC and background rejection rates for two fixed signal efficiencies [2]. We indicate Lorentz-equivariance with an asterisk and estimate uncertainties using five trainings. The first set is trained from scratch, the second using pretraining.

Network	Accuracy	AUC	Time	FLOPs	Memory	Parameters
MIParT-L [26]	0.861	0.9878	43h	225M	53.6G	2380k
LorentzNet* [11]	0.847	0.9856	64h	676M	20.5G	223k
PELICAN-lite*	0.851	0.9862	97h	1370M	27.4G	244k
ParticleNet [9]	0.844	0.9849	25h	413M	16.5G	366k
LLoCa-ParticleNet* [17]	0.848	0.9857	43h	517M	23.5G	385k
ParT [18]	0.861	0.9877	33h	211M	13.3G	2141k
LLoCa-ParT* [17]	0.864	0.9882	66h	315M	19.9G	2160k
Transformer [17]	0.855	0.9867	15h	210M	2.3G	1979k
LLoCa-Transformer* [17]	0.864	0.9882	28h	219M	4.1G	1980k
L-GATr* [16]	0.866	0.9885	166h	2060M	19.0G	1079k
L-GATr-slim*	0.866	0.9885	27h	329M	8.1G	2031k

Table 2: Performance and computational cost for multi-class taggers on the JetClass dataset. We show accuracy, AUC averaged over all pairs of classes, time for a complete training on a H100 GPU, FLOPs per forward pass, maximum memory consumption during training, and number of learnable parameters. Lorentz-equivariant networks are denoted with an asterisk. We use a narrower Frames-Net for the LLoCa-Transformer, because it achieves equal performance at reduced cost.

### 2.3 Amplitude regression

As we view Lorentz-equivariant transformers as tools to construct physics-motivated and efficient latent representations for a broad range of LHC applications, we move to the fully supervised regression of partonic transition amplitudes as a second benchmark task. Partonic transition amplitudes can be expressed analytically and exactly as functions of 4-momenta, but they have to be Lorentz-invariant. Reducing the dimensionality of the input significantly increases the accuracy of the surrogate network, which becomes a key advantage for expensive loop amplitudes and/or amplitudes with many external particles [16, 30–38].

Our benchmark process for amplitude regression is

$$q\bar{q} \rightarrow Z + ng \quad \text{with} \quad n = 1\dots 4, \quad (6)$$

with the acceptance cuts

$$p_T > 20 \text{ GeV} \quad \text{and} \quad \Delta R > 0.4, \quad (7)$$

as described in detail in Ref. [17]. The size of the training dataset is 10M amplitudes. The MSE loss evaluates standardized logarithmic amplitudes over phase space points  $x$ ,

$$\mathcal{L} = |\mathcal{A}_{\text{NN}}(x) - \mathcal{A}_{\text{true}}(x)|^2 \quad \text{with} \quad \mathcal{A}(x) = \frac{\log \mathcal{A}(x) - \overline{\log \mathcal{A}}}{\sigma_{\log \mathcal{A}}}. \quad (8)$$

For simplicity, we use the same MSE as the performance metric for the  $Z + 4$ -gluon case in Tab. 3. In the corresponding Figure we show the same outcome in terms of the relative accuracy

$$\Delta(x) = \frac{\mathcal{A}_{\text{NN}}(x) - \mathcal{A}_{\text{true}}(x)}{\mathcal{A}_{\text{true}}(x)}, \quad (9)$$

histogrammed over an independent test dataset. We compare the Lorentz-equivariant transformer architectures to an MLP with 4-vectors and invariants as input (MLP-I), a standard and a Lorentz-equivariant graph network (GNN and LLoCa-GNN), and a vanilla transformer

Network	MSE $\times 10^{-5}$	FLOPs	Time
MLP-I [16]	$137.0 \pm 2$	0.1M	0.4h
GNN [17]	$10.5 \pm 0.2$	20.7M	0.9h
LLoCa-GNN [17]	$5.0 \pm 0.2$	22.3M	1.5h
Transformer [17]	$8.3 \pm 0.3$	14.9M	1.3h
LLoCa-Transf. [17]	$1.2 \pm 0.2$	16.3M	2.3h
L-GATr [16]	$1.8 \pm 0.2$	528.0M	8.3h
L-GATr-slim	$1.8 \pm 0.1$	23.6M	3.6h

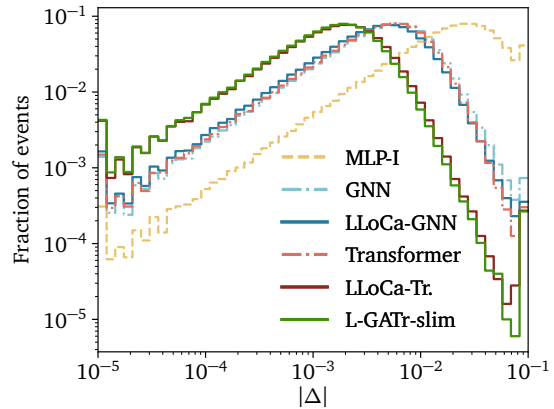


Table 3: Performance for  $Z + 4g$  amplitude regression. Left: MSE performance, cost in terms of FLOPs, and training time on a H100 GPU. Right: relative accuracy over a test dataset. We show error bands based on the standard deviation of three different random seeds.

with 4-vector and PID inputs. As for the other tasks, L-GATr-slim matches the performance of the full L-GATr and the LLoCa-Transformer architectures, outperforming the different graph networks and the vanilla transformer. However, L-GATr-slim requires 20 times fewer training operations and takes less than half of the training time compared to the full L-GATr. With this, L-GATr-slim is almost on par with the resource-efficient and yet accurate LLoCa-Transformer.

## 2.4 Event generation

A third standard task for equivariant transformer representation is the generation of parton-level or jet-level events. Here, a generative network with an equivariant transformer backbone is trained on a set of events from a standard event generator [39–42]. Ideally, the network can then sample more events than it was trained on, and extremely fast [43, 44]. The same kind of event-level generative network is required for neural importance sampling [45–48] and generative unfolding [49–54].

Our benchmark process is two hadronically decaying top quarks in association with up to four extra jets,

$$pp \rightarrow t_h \bar{t}_h + nj, \quad n = 0 \dots 4, \quad (10)$$

described in detail in Ref. [16]. We require exactly two tagged  $b$ -jets and apply the acceptance cuts

$$p_{T,j} > 22 \text{ GeV} \quad \Delta R_{jj} > 0.5 \quad |\eta_j| < 5. \quad (11)$$

Our generative network uses Riemannian flow matching to take into account the phase space topology, and reference vectors to induce symmetry breaking [16]. In the left panel of Fig. 2 we show the negative log-likelihood for all generated events as a function of the training dataset size. As all other shown transformers, L-GATr-slim requires around 500.000 events for optimal performance. The typical percent-level performance in terms of binned standard observables matches the results from Refs. [16, 17]. The right panel of Fig. 2 shows the scaling of the generative network accuracy with the phase space dimension. Again, the performance of L-GATr-slim matches the full L-GATr and the LLoCa-Transformer, with no visible degradation.

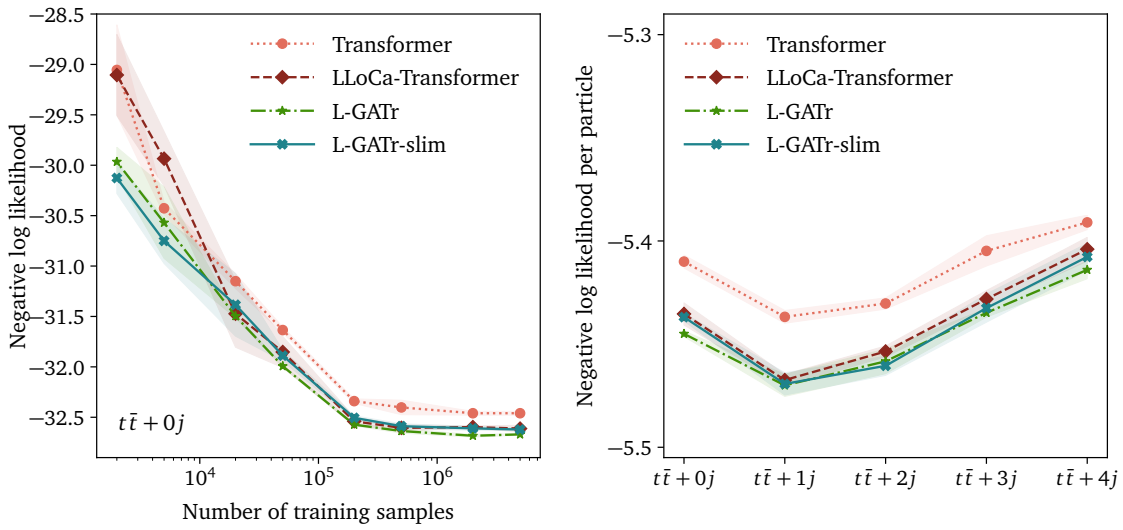


Figure 2: Event generation performance of L-GATr-slim for top pair production with additional jets. We compare it to the original results for L-GATr, Transformer, and LLoCa-Transformer [17].

## 2.5 Ultra-mini taggers

Finally, we study equivariant transformers for much fewer parameters. This downscaling is motivated by the potential use of transformers at different trigger levels, where resources are scarce [55]. This is why we go back to jet tagging to ask what fraction of network parameters we can spare at limited computational cost. We train a standard transformer, ParT, the LLoCa-Transformer, and both L-GATr versions with a decreasing number of 2M, 200k, 20k, and 2k parameters, see App. A. For even smaller parameter numbers we refer to Refs. [56] and [57].

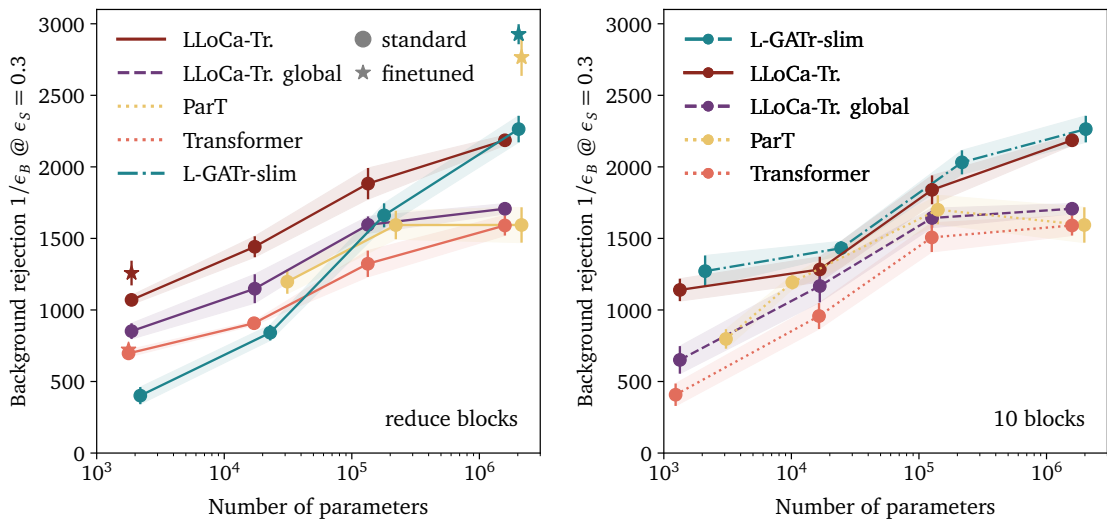


Figure 3: Top taggers with decreasing number of parameter, down to 1000. We decrease the number of blocks from 10 to 4, 2, and 1 (left) or keep them fixed at 10 (right). The left panel includes results for taggers pretrained on the JetClass datasets. ParT requires at least two blocks in the standard implementation, so we do not show a 1000-parameter version.

In the left panel of Fig. 3 we see that when the number of network blocks and width are decreased jointly, the LLoCa-Transformer emerges as the leading architecture at small network sizes. L-GATr-slim falls behind the other networks, because of the limited number of operations that exchange information between the scalar and vector channels. Pretraining on JetClass and fine-tuning on the top-tagging dataset yields a clear performance gain for the 1000-parameter LLoCa Transformer, while the 1000-parameter standard transformer sees only a marginal improvement.

The picture changes in the right panel of Fig. 3, where we keep the number of blocks fixed at 10 and instead reduce the number of parameters per layer. This allows the L-GATr-slim architecture to maintain a background rejection rate above 1000 using only two vector and four scalar channels, marking the leading performance of the 1000-parameter transformer architectures. This shows how we can balance the size and the performance of modern jet taggers, and how the underlying architecture can make a difference in this non-trivial optimization task. For both examples, minimal number of parameters and minimal number of layers, one of the two Lorentz-equivariant architectures works best.

### 3 Quantized jet taggers

The performance of reduced-size taggers motivates further steps to reduce computational cost, specifically for the LLoCa-Transformer tagger. The bottleneck operation in neural networks is typically the linear layer, which involves large matrix multiplications. So-called quantization performs these matrix multiplications at reduced precision, such that they become faster and require less memory. For other network operations reduced precision would hurt performance, so they should be kept at float16 or even float32 precision. We discuss how to quantize four example transformer-based tagging architectures:

- Transformer: vanilla transformer;
- L-GATr-slim: Lorentz-equivariant transformer, using vector and scalar representations;
- LLoCa: Lorentz-equivariant transformer, using Lorentz local canonicalization. We also test a simpler global Lorentz canonicalization.

#### 3.1 Low-precision data types

The speed of GPU operations for all data types has been increasing continuously, as illustrated in Tab. 4. From the rate of this acceleration we see that modern GPUs are increasingly optimized for smaller data types, such as bfloat16 or float8 instead of the established single-precision float32. For scientific applications, most networks are still trained with single precision, i.e. float32. If we want to reduce the computational cost of neural networks, we

	teraFLOPS		
	V100 [58]		A100 [59]
	2017	2020	2022
float64	7	19.5	51
float32	112	156	756
float16/bfloat16	-	312	1513
float8	-	624	3026

Table 4: Floating-point operations per second (FLOPS) for NVIDIA Tensor Core GPUs on different data types.

can first target the data type used throughout the high-dimensional latent space. This can significantly reduce computational cost, while maintaining performance, as demonstrated for bfloat16 [61], float8 [62], and float4 [63].

During training, we apply the automatic mixed precision strategy of using full precision for specific precision-sensitive operations, as well as the backward pass [64]. We do not reduce the precision in input and output layers to enable the network to process and output high-precision numbers. However, we use float8 precision in the linear layers, which dominate the computational cost. To further speed up training, we could perform all operations at lower precision, but would have to use stochastic rounding [65]. In general, the push to lower-dimensional latent representations saturates once the network starts to map out the full range of the provided data type. In practice, this happens around float8 precision [66, 67].

Our implementation emulates low-precision data types in linear layers, because linear layers on float8 are not widely supported yet. We use automatic mixed precision throughout the network and quantize the input of linear layers to the range of float8 values before performing the linear operation in bfloat16 precision. We keep a joint learnable scale parameter in bfloat16 for the final rescaling of the outputs from the float8 range to their original range [66]. Weights are quantized in the same manner. We use straight-through estimation to propagate gradients through this non-differentiable quantization operation. For our three architectures this means:

- Transformer: We first use automatic mixed precision throughout. For all linear layers except the input and output projections, we quantize inputs to float8 using straight-through estimation.
- L-GATr-slim: We apply automatic mixed precision and float8 quantization just as for the transformer.
- LLoCa-Transformer: The LLoCa-Transformer uses the vanilla transformer as its backbone, and we apply automatic mixed precision and float8 quantization accordingly. The linear layers in the Frames-Net are quantized to float8, whereas the orthonormalization procedure is performed in full float32 precision, to avoid numerical symmetry violation. The frame-to-frame transformations in the attention are also performed in float32 precision.

### 3.2 Weight quantization

To reduce the computational cost further we can quantize the linear weights to binary or ternary values, while keeping activations in higher precision [66, 67]. These quantized weights are equipped with a full-precision scale factor that is shared across the full layer. Matrix multiplication with these binary or ternary weights reduces to addition, which can be implemented very efficiently. In addition, quantized weights can be stored more efficiently because of the reduced memory cost.

Quantization-aware training (QAT) is challenging, as gradient descent relies on continuous weight updates, whereas quantized weights inherently lead to non-differentiable losses. We start from a generic loss function and formulate weight quantization as an additional regularization constraint that yields  $R(\theta_k) = 0$  for the quantized parameters,

$$\hat{\theta} = \operatorname{argmin}_{\theta} \mathcal{L}_{\text{QAT}}(\theta) \quad \text{with} \quad \mathcal{L}_{\text{QAT}}(\theta) = \mathcal{L}(\theta) + \lambda \sum_k R(\theta_k). \quad (12)$$

Minimizing this combined loss is impractical. The proximal gradient method instead implements the effect of  $R(\theta_k)$  as a modification to the gradient descent update rule [68], such that

the updated parameters  $\theta'$  minimize Eq. (12). We expand the loss to second order

$$\mathcal{L}(\theta') \approx \mathcal{L}(\theta) + \sum_k \frac{\partial \mathcal{L}(\theta)}{\partial \theta_k} (\theta'_k - \theta_k) + \frac{1}{2} \sum_{k,l} (\theta'_k - \theta_k) \frac{\partial^2 \mathcal{L}(\theta)}{\partial \theta_k \partial \theta_l} (\theta'_l - \theta_l). \quad (13)$$

With the standard Lipschitz assumption for the loss, we can bound the second derivative with a sufficiently large constant  $\kappa$ ,

$$\begin{aligned} \sum_{k,l} (\theta'_k - \theta_k) \frac{\partial^2 \mathcal{L}(\theta)}{\partial \theta_k \partial \theta_l} (\theta'_l - \theta_l) &\leq \kappa |\theta' - \theta|^2 \\ \Rightarrow \mathcal{L}(\theta') &\leq \mathcal{L}(\theta) + \sum_k \frac{\partial \mathcal{L}(\theta)}{\partial \theta_k} (\theta'_k - \theta_k) + \frac{\kappa}{2} |\theta' - \theta|^2 \\ &= \mathcal{L}(\theta) + \frac{\kappa}{2} \sum_k \left[ \theta'_k - \left( \theta_k - \frac{1}{\kappa} \frac{\partial \mathcal{L}(\theta)}{\partial \theta_k} \right) \right]^2 - \frac{1}{2\kappa} \sum_k \left( \frac{\partial \mathcal{L}(\theta)}{\partial \theta_k} \right)^2. \end{aligned} \quad (14)$$

This gives us for the training objective in Eq. (12)

$$\begin{aligned} \hat{\theta}_k &= \operatorname{argmin}_{\theta'_k} \mathcal{L}_{\text{QAT}}(\theta'_k) \\ &= \operatorname{argmin}_{\theta'_k} \left[ \frac{\kappa}{2} \left[ \theta'_k - \left( \theta_k - \frac{1}{\kappa} \frac{\partial \mathcal{L}(\theta)}{\partial \theta_k} \right) \right]^2 + \lambda R(\theta'_k) \right] \\ &= \operatorname{argmin}_{\theta'_k} \left[ \left[ \theta'_k - \left( \theta_k - \frac{1}{\kappa} \frac{\partial \mathcal{L}(\theta)}{\partial \theta_k} \right) \right]^2 + \frac{2\lambda}{\kappa} R(\theta'_k) \right], \end{aligned} \quad (15)$$

because adding and multiplying constants do not change the result of  $\operatorname{argmin}$ . The first term describes the standard gradient descent for  $\mathcal{L}(\theta)$  with a learning rate  $1/\kappa$ , leading to the naive parameter update

$$\tilde{\theta}_k = \theta_k - \frac{1}{\kappa} \frac{\partial \mathcal{L}(\theta)}{\partial \theta_k}. \quad (16)$$

We now define the proximal operator as a post-hoc modification of this update rule that yields the optimally updated parameters  $\hat{\theta}$  from Eq. (12),

$$\begin{aligned} \hat{\theta}_k &= \operatorname{prox}_R(\tilde{\theta}_k) \\ &\equiv \operatorname{argmin}_{\theta'_k} \left[ (\theta'_k - \tilde{\theta}_k)^2 + \frac{2\lambda}{\kappa} R(\theta'_k) \right]. \end{aligned} \quad (17)$$

Instead of directly using the result from naive gradient descent  $\tilde{\theta}_k$  to update the network parameters as  $\theta'_k = \tilde{\theta}_k$ , the proximal operator performs a post-processing on  $\tilde{\theta}_k$  to account for the regularization term, with  $\lambda/\kappa$  being a measure of the regularization strength.

An efficient implementation requires a closed form for the proximal operator. We write the regularization term as a piecewise-affine regularizer (PAR) [69],

$$R(\theta_k) \Big|_{\text{PAR}} = \max_i [a_i (|\theta_k| - q_i) + b_i]. \quad (18)$$

The slopes satisfy  $0 \leq a_0 < a_1 < \dots < a_m = \infty$ , and for the quantized values  $\{0, \pm q_1, \dots, \pm q_m\}$  the biases become

$$b_0 = 0 \quad \text{and} \quad b_i = b_{i-1} + a_{i-1} (q_i - q_{i-1}). \quad (19)$$

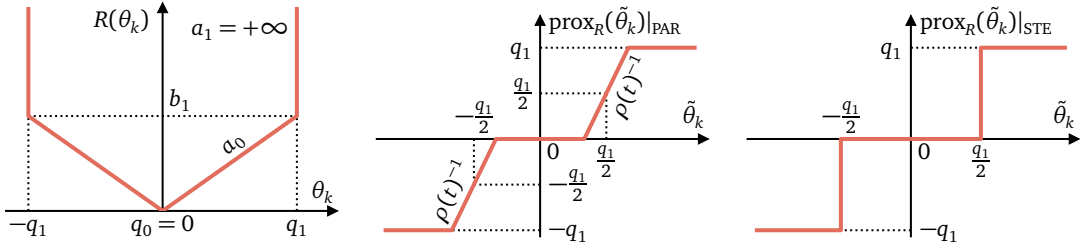


Figure 4: Regularizer function  $R(\theta_k)$  for ternary quantization (left), proximal map  $\text{prox}_R(\tilde{\theta}_k)$  for soft quantization at time  $t$  (middle), and final proximal map for hard quantization (right). The proximal map parametrized by  $\rho(t)$  corresponds to the regularizer function defined with  $a_0 = (1 + \rho(t))q_1/2$  and  $b_1 = a_0 q_1$ .

This form for  $R(\theta_k)$  is visualized in Fig. 4. The proximal operator has a closed form

$$\text{prox}_R(\tilde{\theta}_k) \Big|_{\text{PAR}} = \begin{cases} \text{sign}(\tilde{\theta}_k)q_i & |\tilde{\theta}_k| \in [a_{i-1} + q_i, a_i + q_i] \\ \tilde{\theta}_k - \text{sign}(\tilde{\theta}_k)a_i & |\tilde{\theta}_k| \in [a_i + q_i, a_i + q_{i+1}] \end{cases}. \quad (20)$$

We choose the parameters  $\{a_i\}_{0 \leq i \leq m}$  such that the slopes of the proximal map affine pieces are defined by a single parameter  $\rho(t)$  depending on time or iteration count [69]

$$a_i = \frac{1 + \rho(t)}{2}q_{i+1} + \frac{1 - \rho(t)}{2}q_i. \quad (21)$$

The parameter  $\rho(t)$  corresponds to the inverse slope of the proximal map non-horizontal segments. During training, it is annealed from one to zero, with a sigmoid-like scheduler. This way the proximal map smoothly transitions from the identity to a step function, and the weights are progressively quantized. The evolution of the proximal map is illustrated in Fig. 4.

A straightforward quantization-aware training, straight-through estimation (STE), is a special case of the proximal gradient formalism where the regularizer consists of delta distributions, with a step-function as the proximal map. It is equivalent to replacing the annealing schedule with  $\rho(t) = 0$ .

$$\begin{aligned} R(\theta_k) \Big|_{\text{STE}} &= \sum_i [\delta(\theta_k - q_i) + \delta(\theta_k + q_i)] \\ \text{prox}_R(\tilde{\theta}_k) \Big|_{\text{STE}} &= \text{sign}(\tilde{\theta}_k)q_k. \end{aligned} \quad (22)$$

We compare PARQ and STE for our applications and typically find that PARQ stabilizes training and achieves marginally better performance.

We use weight quantization for the same linear layers that use low-precision data types described in Sec. 3.1, with the exception of the LLoCa-Transformer Frames-Net where we keep weights at the same precision as the inputs. The fraction of quantized weights varies between 90% and 99% for the different architectures and numbers of parameters.

### 3.3 Quantized equivariant taggers

First, we compare quantization-aware training with PARQ and with the naive STE in Tab. 5. The vanilla transformer maintains performance up to float8 precision, but drops in performance after weight quantization. In contrast, all networks using Lorentz equivariance maintain constant performance when quantized. Here, it is important to ensure that weight quantization and input quantization violate the Lorentz only equivariance in a minimal way. For

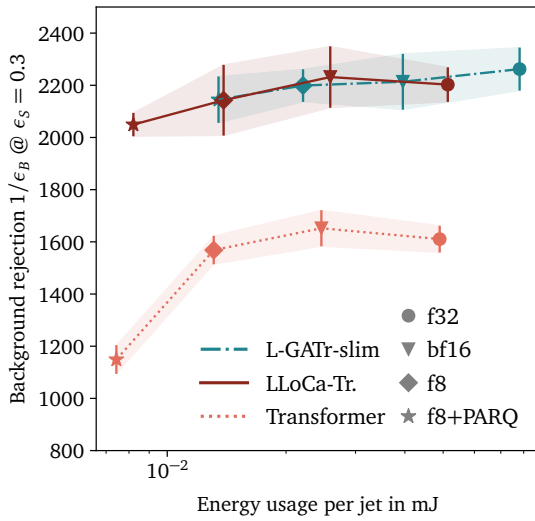


Figure 5: Energy consumption per jet using different taggers and quantization approaches. We have old (left) and new but in process (right).

the LLoCa-Transformer, we perform the equivariance-critical orthonormalization and the projection into the local frames in full precision, and limit low-precision operations to Lorentz-invariants. For L-GATr-slim, we multiply full vectors with quantized weights, which again does not incur any additional Lorentz violation. Nevertheless, our quantized LLoCa-Transformer and L-GATr-slim can only satisfy Lorentz-equivariance to the precision of the linear layer inputs, which are float8, translating into violation effects at the 10% level. We find that this violation does not translate into significant drops in performance.

For top tagging with resource-efficient networks we estimate the energy use. An H100 has a maximum power consumption of  $P = 350$  W for the throughput in teraFLOPS  $T$  given in Tab. 4. We estimate the energy use per operation as  $E = T/P$  for each data type and the total energy consumption of a forward pass by counting all operations in the network and weighting them with the corresponding energy cost [70]. For a conservative estimate, we assume that addition and multiplication consume the same amount of energy, effectively reducing the computational cost of linear operations of a float8 latent representation with ternary weights by a factor of two compared to float8-precision weights which also require a multiplication.

Next, we correlate the energy consumption with the performance of different quantized taggers in Fig. 5. Our estimates for the energy cost indicate that every quantization step reduces the cost by a factor of about two, accumulating to an almost order-of-magnitude gain when combining all steps. L-GATr-slim consumes about 50% more energy than a vanilla transformer due to its more expensive linear layers, whereas the LLoCa Transformer incurs a negligible additional energy cost. Importantly, these energy savings come at no performance loss,

	Background rejection $1/\epsilon_B @ \epsilon_S = 0.3$			
	fp32	fp8	fp8+STE	fp8+PARQ
Transformer	$1613 \pm 118$	$1568 \pm 54$	$1186 \pm 41$	$1149 \pm 55$
LLoCa-Transformer	$2150 \pm 130$	$2142 \pm 136$	$2024 \pm 155$	$2049 \pm 45$
L-GATr-slim	$2264 \pm 93$	$2199 \pm 62$	$2023 \pm 102$	$2145 \pm 89$

Table 5: Impact of different kinds of input and weight quantization on network performance

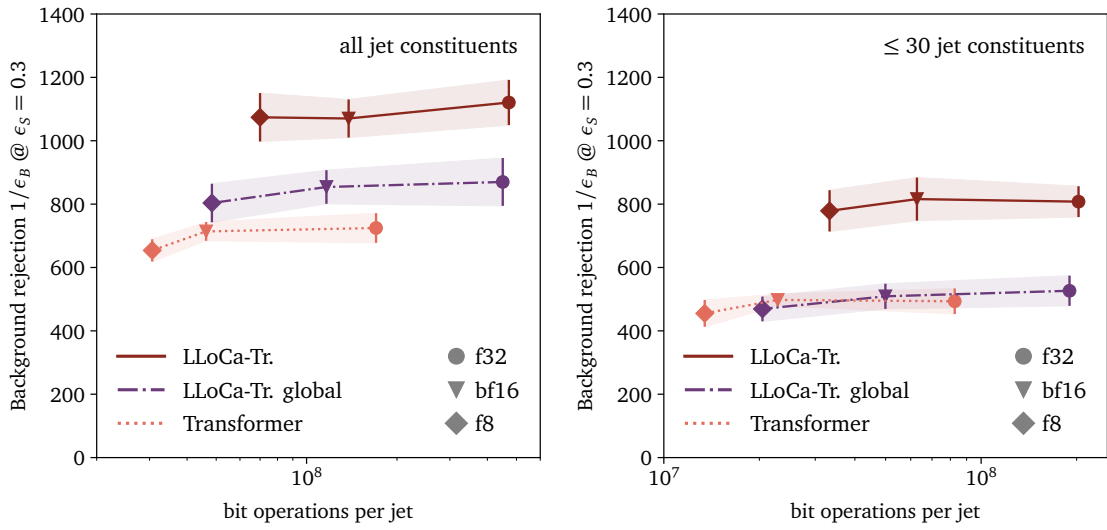


Figure 6: Number of bit-operations per jet for different taggers and quantization approaches, using the full range of jet constituents (left) and only up to 30 constituents (right).

they only require the implementation of optimized low-precision operations.

### 3.4 Towards online jet tagging

An exciting question is whether small and quantized transformers can meet the resource and latency requirements of FPGAs. In that case, resource-efficient version of the leading jet taggers can be applied at the trigger level. Information about the partonic nature of a jet would open entirely new avenues for HL-LHC analyses. The state-of-the-art approach to FPGA-ready networks is high granularity quantization (HGQ) [71], where we learn the bit-width of each operation using backpropagation. Since this study can only serve as a first proof of principle, we use GPU implementations instead of an FPGA, as well as our naive fp8 quantization instead of HGQ.

For this test, we reduce a naive transformer and the LLoCa-Transformer to one block and a, typically, 16-dimensional latent space. Even for low numerical precision the orthonormalization has to be done to full precision, so its cost is significant. Therefore, we also show results for the global canonicalization LLoCa-Transformer, which requires the orthonormalization only for one particle and does not involve frame-to-frame conversions. From Fig. 3 we know that L-GATr and L-GATr-slim show poor performance for a minimal number of blocks. Adding more blocks solves this problem, but significantly increases the latency, so we omit the L-GATr architecture for now. The results are shown in Fig. 6. In the left panel we see that, as before, we can reduce the numerical precision without significant performance drop, down to float8.

In the right panel of Fig. 6 we reduce the input data from up to the full set of particle-flow constituents to 30 at most. Depending on the transverse momentum the number of constituents inside a top jet peaks above 50 [10]. This means that while the general picture does not change, the performance of the top taggers decreases significantly when we only consider the leading 30 constituents.

## 4 Outlook

As for industry applications, upscaled transformers are currently driving the performance frontier for jet tagging as the leading ML-application in LHC physics. However, this performance gain comes with an over-proportional compute cost in training and evaluation. For dedicated physics applications, we studied the opposite approach, physics-aware downscaling of transformers, in terms of network parameters and using quantized parameters.

As a starting point, we have presented an efficient version of the equivariant L-GATr architecture, L-GATr-slim. It constructs powerful latent representations for many LHC tasks, from jet tagging to amplitude regression and event generation. Compared to L-GATr, we reduced the training time by a factor six and the memory footprint by a factor 2.3, at no cost in tagging performance. In this way, the geometric algebra approach is competitive with the local canonicalization, specifically the LLoCa-Transformer.

For L-GATr-slim and LLoCa we then tested the performance down to 1k network parameters, either reducing the number of layers or reducing the number of parameters per layer. While this down-scaling comes with a reduced performance, the LLoCa-Transformer remains a powerful tool for a small number of blocks, while L-GATr-slim leads the competition for a fixed number of blocks and a reduced number of parameters per block.

To further improve efficiency, we quantized the network parameters using the standard PARQ and STE methods. The inductive bias from Lorentz equivariance prevents a performance drop from this weight quantization, such that the performance of the LLoCa-Transformer and L-GATr-slim are unaffected by input and by weight quantization. Here, it is crucial that we ensure that the weight quantization does not affect the Lorentz equivariance significantly.

Finally, we have combined size-reduction and quantization strategies to construct a minimal Lorentz-equivariant tagger, with the ultimate goal of jet tagging at the trigger level. Even though the FPGA-inspired minimal LLoCa-Transformer loses a factor of two in background rejection compared to its full-size counterpart, it still outperforms all pre-graph top taggers [2].

### Code availability

Our code is available at <https://github.com/heidelberg-hepml/tagger-quantization>. The amplitude regression and event generation experiments were performed using <https://github.com/heidelberg-hepml/lloca-experiments>. L-GATr-slim is available as part of the L-GATr package <https://github.com/heidelberg-hepml/lgatr>.

### Acknowledgements

We would like to thank Thea Arrestad for expert advice on FPGAs and to Luigi Favaro, Víctor Bresó Pla, and Huilin Qu for many helpful discussions. This work is supported by the Deutsche Forschungsgemeinschaft (DFG, German Research Foundation) under grant 396021762 – TRR 257 *Particle Physics Phenomenology after the Higgs Discovery*. It has received funding from the European Union’s Horizon Europe research and innovation programme under the Marie Skłodowska-Curie grant agreement No 101168829, *Challenging AI with Challenges from Physics: How to solve fundamental problems in Physics by AI and vice versa* (AIPHY). JS is supported by the Humboldt Foundation through a Feodor-Lynen Fellowship. The authors acknowledge support by the state of Baden-Württemberg through bwHPC and the German Research Foundation (DFG) through the grants INST 35/1597-1 FUGG and INST 39/1232-1 FUGG. This

work made use of the facilities of the N8 Centre of Excellence in Computationally Intensive Research (N8 CIR) provided and funded by the N8 research partnership and EPSRC (Grant No. EP/T022167/1). The Centre is coordinated by the Universities of Durham, Manchester and York.

## A Implementation details

We use the github repositories <https://github.com/heidelberg-hepml/tagger-quantization> for jet tagging, and <https://github.com/heidelberg-hepml/lloca-experiments> for amplitude regression and event generation. All hyperparameter choices can be found in the config/ folders which is present in both repositories, and the file REPRODUCE.md contains the commands to reproduce all results given in this paper.

### Jet tagging

Our LLoCa-Transformer closely follows Ref. [17], with a smaller Frames-Net that uses 32 instead of 128 hidden channels in the MLP. We find that this setting achieves the same performance, but reduces FLOPs and memory use significantly.

Our L-GATr-slim tagger uses 12 blocks, 32 vector channels, 96 scalar channels, and 8 attention heads. It is trained for 200k iterations on the top tagging dataset, using the Lion optimizer with batch size 128, learning rate  $3 \times 10^{-5}$ , weight decay 2, and a cosine annealing learning rate schedule. The JetClass training uses 1M iterations, and using the same optimizer, batch size, learning rate, and learning rate schedule as ParT, see Ref. [18]. To finetune a L-GATr-slim tagger that was pretrained on the JetClass dataset using the same training setup, we use the training setup described above with a learning rate of  $3 \times 10^{-6}$  for the transformer backbone, and a learning rate of  $3 \times 10^{-4}$  for the final linear layer.

### Amplitude regression

Our L-GATr-slim amplitude regressor is designed to closely follow the shape of the L-GATr amplitude regressor in Ref. [17], with 8 blocks, 40 vector channels, 72 scalar channels, and 8 heads. It follows the training setup used for all amplitude networks in Ref. [17], with 200k iterations, Adam optimizer, batch size 1024, learning rate  $10^{-3}$ , and a step-wise learning rate reduction whenever the loss saturates.

### Event generation

The L-GATr-slim event generator closely follows the L-GATr event generator in Ref. [16], which 6 blocks, 32 vector channels, 64 scalar channels, and 8 heads. It uses the same training setup with 200k iterations, AdamW optimizer, batch size 2048, and learning rate  $10^{-3}$ , and a step-wise learning rate reduction whenever the loss saturates.

### Ultra-mini taggers

For each network in Fig. 3, we provide the hyperparameters of the architecture in Table 6. The deep models correspond to the right plot. We use different training hyperparameters for each network size, given in Table 7. All networks are trained for 200 000 iterations using the

Architecture	2M	200k	20k	2k	200k (deep)	20k (deep)	2k (deep)
Transformer	channels	128/256	64/128	32/64	16/32	32/64	16/16
	heads	8	4	4	2	4	2
	blocks	12	4	2	1	10	10
FramesNet (LLoCa)	channels	32	16	8	4	16	8
	layers	2	2	2	2	2	2
	channels	128/512	64/128	32/64	—	32/128	8/16
ParT	pair chan.	64	16	8	—	16	4
	heads	8	4	2	—	4	1
	blocks	8+2	3+1	1+1	—	8+2	8+2
L-GATr-slim	vectors	32/128	16/32	8/16	4/4	8/32	4/4
	scalars	96/384	64/128	32/64	16/16	32/128	16/16
	heads	8	4	4	2	4	2
	blocks	12	4	2	1	10	10

Table 6: Architecture hyperparameters for the different taggers of Fig. 3.

Configuration	200k	20k	2k
Batchsize	256	512	4096
Learning Rate	$10^{-3}$	$3 \times 10^{-3}$	$10^{-2}$
Weight Decay	0.1	0	0

Table 7: Training hyperparameters for the different taggers of Fig. 3. The same hyperparameters are used for the deep and shallow models.

Adam optimizer with a cosine-annealing learning rate schedule. We use the same training hyperparameters for the deep and shallow networks.

## References

- [1] T. Plehn, A. Butter, B. Dillon, T. Heimel, C. Krause, and R. Winterhalder, *Modern Machine Learning for LHC Physicists*, arXiv:2211.01421 [hep-ph].
- [2] A. Butter *et al.*, *The Machine Learning landscape of top taggers*, SciPost Phys. **7** (2019) 014, arXiv:1902.09914 [hep-ph].
- [3] B. Nachman *et al.*, *Jets and Jet Substructure at Future Colliders*, Front. in Phys. **10** (2022) 897719, arXiv:2203.07462 [hep-ph].
- [4] J. Cogan, M. Kagan, E. Strauss, and A. Schwartzman, *Jet-Images: Computer Vision Inspired Techniques for Jet Tagging*, JHEP **02** (2015) 118, arXiv:1407.5675 [hep-ph].
- [5] P. Baldi, P. Sadowski, and D. Whiteson, *Searching for Exotic Particles in High-Energy Physics with Deep Learning*, Nature Commun. **5** (2014) 4308, arXiv:1402.4735 [hep-ph].
- [6] L. de Oliveira, M. Kagan, L. Mackey, B. Nachman, and A. Schwartzman, *Jet-images — deep learning edition*, JHEP **07** (2016) 069, arXiv:1511.05190 [hep-ph].

- [7] J. Gallicchio and M. D. Schwartz, *Seeing in Color: Jet Superstructure*, *Phys. Rev. Lett.* **105** (2010) 022001, [arXiv:1001.5027 \[hep-ph\]](https://arxiv.org/abs/1001.5027).
- [8] G. Kasieczka, T. Plehn, M. Russell, and T. Schell, *Deep-learning Top Taggers or The End of QCD?*, *JHEP* **05** (2017) 006, [arXiv:1701.08784 \[hep-ph\]](https://arxiv.org/abs/1701.08784).
- [9] H. Qu and L. Gouskos, *ParticleNet: Jet Tagging via Particle Clouds*, *Phys. Rev. D* **101** (2020) 5, 056019, [arXiv:1902.08570 \[hep-ph\]](https://arxiv.org/abs/1902.08570).
- [10] A. Butter, G. Kasieczka, T. Plehn, and M. Russell, *Deep-learned Top Tagging with a Lorentz Layer*, *SciPost Phys.* **5** (2018) 3, 028, [arXiv:1707.08966 \[hep-ph\]](https://arxiv.org/abs/1707.08966).
- [11] S. Gong, Q. Meng, J. Zhang, H. Qu, C. Li, S. Qian, W. Du, Z.-M. Ma, and T.-Y. Liu, *An efficient Lorentz equivariant graph neural network for jet tagging*, *JHEP* **07** (2022) 030, [arXiv:2201.08187 \[hep-ph\]](https://arxiv.org/abs/2201.08187).
- [12] S. Qiu, S. Han, X. Ju, B. Nachman, and H. Wang, *Holistic approach to predicting top quark kinematic properties with the covariant particle transformer*, *Phys. Rev. D* **107** (2023) 11, 114029, [arXiv:2203.05687 \[hep-ph\]](https://arxiv.org/abs/2203.05687).
- [13] A. Bogatskiy, T. Hoffman, D. W. Miller, and J. T. Offermann, *PELICAN: Permutation Equivariant and Lorentz Invariant or Covariant Aggregator Network for Particle Physics*, [arXiv:2211.00454 \[hep-ph\]](https://arxiv.org/abs/2211.00454).
- [14] S. Qiu, S. Han, X. Ju, B. Nachman, and H. Wang, *Parton labeling without matching: unveiling emergent labelling capabilities in regression models*, *Eur. Phys. J. C* **83** (2023) 7, 622, [arXiv:2304.09208 \[hep-ph\]](https://arxiv.org/abs/2304.09208).
- [15] D. Ruhe, J. Brandstetter, and P. Forré, *Clifford group equivariant neural networks*, in *Advances in Neural Information Processing Systems*. 5, 2023. [arXiv:2305.11141 \[cs.LG\]](https://arxiv.org/abs/2305.11141).
- [16] J. Brehmer, V. Bresó, P. de Haan, T. Plehn, H. Qu, J. Spinner, and J. Thaler, *A Lorentz-equivariant transformer for all of the LHC*, *SciPost Phys.* **19** (2025) 4, 108, [arXiv:2411.00446 \[hep-ph\]](https://arxiv.org/abs/2411.00446).
- [17] L. Favaro, G. Gerhartz, F. A. Hamprecht, P. Lippmann, S. Pitz, T. Plehn, H. Qu, and J. Spinner, *Lorentz-Equivariance without Limitations*, [arXiv:2508.14898 \[hep-ph\]](https://arxiv.org/abs/2508.14898).
- [18] H. Qu, C. Li, and S. Qian, *Particle Transformer for Jet Tagging*, [arXiv:2202.03772 \[hep-ph\]](https://arxiv.org/abs/2202.03772).
- [19] W. Bhimji, C. Harris, V. Mikuni, and B. Nachman, *OmniLearned: A Foundation Model Framework for All Tasks Involving Jet Physics*, [arXiv:2510.24066 \[hep-ph\]](https://arxiv.org/abs/2510.24066).
- [20] J. Birk, A. Hallin, G. Kasieczka, N. Madzharova, I. Pang, and D. Shih, *Enhancing next token prediction based pre-training for jet foundation models*, [arXiv:2512.04149 \[hep-ph\]](https://arxiv.org/abs/2512.04149).
- [21] V. Loncar *et al.*, *Compressing deep neural networks on FPGAs to binary and ternary precision with HLS4ML*, *Mach. Learn. Sci. Tech.* **2** (2021) 015001, [arXiv:2003.06308 \[cs.LG\]](https://arxiv.org/abs/2003.06308).
- [22] B. Hawks, J. Duarte, N. J. Fraser, A. Pappalardo, N. Tran, and Y. Umuroglu, *Ps and Qs: Quantization-aware pruning for efficient low latency neural network inference*, [arXiv:2102.11289 \[cs.LG\]](https://arxiv.org/abs/2102.11289).

- [23] C. Krause, D. Wang, and R. Winterhalder, *BitHEP – The Limits of Low-Precision ML in HEP*, [arXiv:2504.03387 \[hep-ph\]](https://arxiv.org/abs/2504.03387).
- [24] S. Rai, Prisha, and J. Kumar, *Investigating 1-Bit Quantization in Transformer-Based Top Tagging*, [arXiv:2508.07431 \[hep-ph\]](https://arxiv.org/abs/2508.07431).
- [25] Y. N. Dauphin, A. Fan, M. Auli, and D. Grangier, *Language modeling with gated convolutional networks*, in *Proceedings of the 34th International Conference on Machine Learning (ICML)*. PMLR, 2017.
- [26] Y. Wu, K. Wang, C. Li, H. Qu, and J. Zhu, *Jet Tagging with More-Interaction Particle Transformer*, [arXiv:2407.08682 \[hep-ph\]](https://arxiv.org/abs/2407.08682).
- [27] W. Esmail, A. Hammad, and M. Nojiri, *IAFormer: Interaction-Aware Transformer network for collider data analysis*, [arXiv:2505.03258 \[hep-ph\]](https://arxiv.org/abs/2505.03258).
- [28] A. Bogatskiy, T. Hoffman, D. W. Miller, J. T. Offermann, and X. Liu, *Explainable equivariant neural networks for particle physics: PELICAN*, [JHEP 03 \(2024\) 113](https://doi.org/10.1007/JHEP03(2024)113), [arXiv:2307.16506 \[hep-ph\]](https://arxiv.org/abs/2307.16506).
- [29] V. Mikuni and B. Nachman, *Solving key challenges in collider physics with foundation models*, [Phys. Rev. D 111 \(2025\) 5, L051504](https://doi.org/10.1103/PhysRevD.111.L051504), [arXiv:2404.16091 \[hep-ph\]](https://arxiv.org/abs/2404.16091).
- [30] J. Aylett-Bullock, S. Badger, and R. Moodie, *Optimising simulations for diphoton production at hadron colliders using amplitude neural networks*, [JHEP 08 \(6, 2021\) 066](https://doi.org/10.1007/JHEP08(2021)066), [arXiv:2106.09474 \[hep-ph\]](https://arxiv.org/abs/2106.09474).
- [31] D. Maître and H. Truong, *A factorisation-aware Matrix element emulator*, [JHEP 11 \(7, 2021\) 066](https://doi.org/10.1007/JHEP11(2021)066), [arXiv:2107.06625 \[hep-ph\]](https://arxiv.org/abs/2107.06625).
- [32] S. Badger, A. Butter, M. Luchmann, S. Pitz, and T. Plehn, *Loop amplitudes from precision networks*, [SciPost Phys. Core 6 \(2023\) 034](https://doi.org/10.21468/SciPostPhysCore.6.034), [arXiv:2206.14831 \[hep-ph\]](https://arxiv.org/abs/2206.14831).
- [33] D. Maître and H. Truong, *One-loop matrix element emulation with factorisation awareness*, [arXiv:2302.04005 \[hep-ph\]](https://arxiv.org/abs/2302.04005).
- [34] V. Bresó, G. Heinrich, V. Magerya, and A. Olsson, *Interpolating amplitudes*, [arXiv:2412.09534 \[hep-ph\]](https://arxiv.org/abs/2412.09534).
- [35] H. Bahl, N. Elmer, L. Favaro, M. Haußmann, T. Plehn, and R. Winterhalder, *Accurate Surrogate Amplitudes with Calibrated Uncertainties*, [SciPost Phys. Core 8 \(2025\) 073](https://doi.org/10.21468/SciPostPhysCore.8.073), [arXiv:2412.12069 \[hep-ph\]](https://arxiv.org/abs/2412.12069).
- [36] H. Bahl, N. Elmer, T. Plehn, and R. Winterhalder, *Amplitude Uncertainties Everywhere All at Once*, [arXiv:2509.00155 \[hep-ph\]](https://arxiv.org/abs/2509.00155).
- [37] J. M. Villadamigo, R. Frederix, T. Plehn, T. Vitos, and R. Winterhalder, *FASTColor – Full-color Amplitude Surrogate Toolkit for QCD*, [arXiv:2509.07068 \[hep-ph\]](https://arxiv.org/abs/2509.07068).
- [38] L. Beccatini, F. Maltoni, O. Mattelaer, and R. Winterhalder, *Amplitude Surrogates for Multi-Jet Processes*, [arXiv:2512.11036 \[hep-ph\]](https://arxiv.org/abs/2512.11036).
- [39] A. Butter, T. Plehn, and R. Winterhalder, *How to GAN LHC Events*, [SciPost Phys. 7 \(2019\) 6, 075](https://doi.org/10.21468/SciPostPhys.7.6.075), [arXiv:1907.03764 \[hep-ph\]](https://arxiv.org/abs/1907.03764).

[40] A. Butter, T. Heimel, S. Hummerich, T. Krebs, T. Plehn, A. Rousselot, and S. Vent, *Generative networks for precision enthusiasts*, *SciPost Phys.* **14** (2023) 4, 078, [arXiv:2110.13632 \[hep-ph\]](https://arxiv.org/abs/2110.13632).

[41] A. Butter, N. Huetsch, S. Palacios Schweitzer, T. Plehn, P. Sorrenson, and J. Spinner, *Jet diffusion versus JetGPT – Modern networks for the LHC*, *SciPost Phys. Core* **8** (2025) 026, [arXiv:2305.10475 \[hep-ph\]](https://arxiv.org/abs/2305.10475).

[42] A. Butter, F. Charton, J. M. Villadamigo, A. Ore, T. Plehn, and J. Spinner, *Extrapolating Jet Radiation with Autoregressive Transformers*, [arXiv:2412.12074 \[hep-ph\]](https://arxiv.org/abs/2412.12074).

[43] A. Butter, S. Diefenbacher, G. Kasieczka, B. Nachman, and T. Plehn, *GANplifying event samples*, *SciPost Phys.* **10** (2021) 6, 139, [arXiv:2008.06545 \[hep-ph\]](https://arxiv.org/abs/2008.06545).

[44] H. Bahl, S. Diefenbacher, N. Elmer, T. Plehn, and J. Spinner, *Forecasting Generative Amplification*, [arXiv:2509.08048 \[hep-ph\]](https://arxiv.org/abs/2509.08048).

[45] C. Gao, J. Isaacson, and C. Krause, *i-flow: High-dimensional Integration and Sampling with Normalizing Flows*, *Mach. Learn. Sci. Tech.* **1** (1, 2020) 045023, [arXiv:2001.05486 \[physics.comp-ph\]](https://arxiv.org/abs/2001.05486).

[46] E. Bothmann, T. Janßen, M. Knobbe, T. Schmale, and S. Schumann, *Exploring phase space with Neural Importance Sampling*, *SciPost Phys.* **8** (1, 2020) 069, [arXiv:2001.05478 \[hep-ph\]](https://arxiv.org/abs/2001.05478).

[47] T. Heimel, R. Winterhalder, A. Butter, J. Isaacson, C. Krause, F. Maltoni, O. Mattelaer, and T. Plehn, *MadNIS - Neural multi-channel importance sampling*, *SciPost Phys.* **15** (2023) 4, 141, [arXiv:2212.06172 \[hep-ph\]](https://arxiv.org/abs/2212.06172).

[48] T. Heimel, N. Huetsch, F. Maltoni, O. Mattelaer, T. Plehn, and R. Winterhalder, *The MadNIS reloaded*, *SciPost Phys.* **17** (2024) 1, 023, [arXiv:2311.01548 \[hep-ph\]](https://arxiv.org/abs/2311.01548).

[49] M. Bellagente, A. Butter, G. Kasieczka, T. Plehn, and R. Winterhalder, *How to GAN away Detector Effects*, *SciPost Phys.* **8** (2020) 4, 070, [arXiv:1912.00477 \[hep-ph\]](https://arxiv.org/abs/1912.00477).

[50] M. Bellagente, A. Butter, G. Kasieczka, T. Plehn, A. Rousselot, R. Winterhalder, L. Ardizzone, and U. Köthe, *Invertible Networks or Partons to Detector and Back Again*, *SciPost Phys.* **9** (2020) 074, [arXiv:2006.06685 \[hep-ph\]](https://arxiv.org/abs/2006.06685).

[51] S. Diefenbacher, G.-H. Liu, V. Mikuni, B. Nachman, and W. Nie, *Improving Generative Model-based Unfolding with Schrödinger Bridges*, [arXiv:2308.12351 \[hep-ph\]](https://arxiv.org/abs/2308.12351).

[52] N. Huetsch *et al.*, *The landscape of unfolding with machine learning*, *SciPost Phys.* **18** (2025) 2, 070, [arXiv:2404.18807 \[hep-ph\]](https://arxiv.org/abs/2404.18807).

[53] A. Butter, T. Heimel, N. Huetsch, M. Kagan, and T. Plehn, *Simulation-Prior Independent Neural Unfolding Procedure*, [arXiv:2507.15084 \[hep-ph\]](https://arxiv.org/abs/2507.15084).

[54] A. Petitjean, A. Butter, K. Greif, S. Palacios Schweitzer, T. Plehn, J. Spinner, and D. Whiteson, *Generative Unfolding of Jets and Their Substructure*, [arXiv:2510.19906 \[hep-ph\]](https://arxiv.org/abs/2510.19906).

[55] P. Odagiu *et al.*, *Ultrafast jet classification at the HL-LHC*, *Mach. Learn. Sci. Tech.* **5** (2024) 3, 035017, [arXiv:2402.01876 \[hep-ex\]](https://arxiv.org/abs/2402.01876).

[56] A. Bogatskiy, T. Hoffman, and J. T. Offermann, *19 Parameters Is All You Need: Tiny Neural Networks for Particle Physics*, [arXiv:2310.16121 \[hep-ph\]](https://arxiv.org/abs/2310.16121).

[57] S. Vent, R. Winterhalder, and T. Plehn, *How to Deep-Learn the Theory behind Quark-Gluon Tagging*, [arXiv:2507.21214 \[hep-ph\]](https://arxiv.org/abs/2507.21214).

[58] NVIDIA Corporation, “NVIDIA V100 tensor core GPU datasheet.” Online datasheet, 2020. Accessed 10 Dec 2025.

[59] NVIDIA Corporation, “NVIDIA A100 tensor core GPU datasheet.” Online datasheet, 2022. Accessed 10 Dec 2025.

[60] NVIDIA Corporation, “NVIDIA H100 tensor core GPU datasheet.” Online datasheet, 2024. Accessed 10 Dec 2025.

[61] D. Kalamkar, D. Mudigere, N. Mellemundi, D. Das, K. Banerjee, S. Avancha, D. T. Vooturi, N. Jammalamadaka, J. Huang, H. Yuen, *et al.*, *A study of bfloat16 for deep learning training*, [arXiv:1905.12322 \[cs.LG\]](https://arxiv.org/abs/1905.12322).

[62] P. Micikevicius, D. Stolic, N. Burgess, M. Cornea, P. Dubey, R. Grisenthwaite, S. Ha, A. Heinecke, P. Judd, J. Kamalu, *et al.*, *Fp8 formats for deep learning*, [arXiv:2209.05433 \[cs.LG\]](https://arxiv.org/abs/2209.05433).

[63] S.-y. Liu, Z. Liu, X. Huang, P. Dong, and K.-T. Cheng, *Llm-fp4: 4-bit floating-point quantized transformers*, [arXiv:2310.16836 \[cs.LG\]](https://arxiv.org/abs/2310.16836).

[64] P. Micikevicius, S. Narang, J. Alben, G. Diamos, E. Elsen, D. Garcia, B. Ginsburg, M. Houston, O. Kuchaiev, G. Venkatesh, *et al.*, *Mixed precision training*, [arXiv:1710.03740 \[cs.LG\]](https://arxiv.org/abs/1710.03740).

[65] S. Gupta, A. Agrawal, K. Gopalakrishnan, and P. Narayanan, *Deep learning with limited numerical precision*, [arXiv:1502.02551 \[cs.LG\]](https://arxiv.org/abs/1502.02551).

[66] H. Wang, S. Ma, L. Dong, S. Huang, H. Wang, L. Ma, F. Yang, R. Wang, Y. Wu, and F. Wei, *Bitnet: Scaling 1-bit transformers for large language models*, [arXiv:2310.11453 \[cs.LG\]](https://arxiv.org/abs/2310.11453).

[67] S. Ma, H. Wang, L. Ma, L. Wang, W. Wang, S. Huang, L. Dong, R. Wang, J. Xue, and F. Wei, *The era of 1-bit llms: All large language models are in 1.58 bits*, [arXiv:2402.17764 \[cs.LG\]](https://arxiv.org/abs/2402.17764).

[68] Y. Bai, Y.-X. Wang, and E. Liberty, *Proxquant: Quantized neural networks via proximal operators*, [arXiv:1810.00861 \[cs.LG\]](https://arxiv.org/abs/1810.00861).

[69] L. Jin, J. Ma, Z. Liu, A. Gromov, A. Defazio, and L. Xiao, *Parq: Piecewise-affine regularized quantization*, [arXiv:2503.15748 \[cs.LG\]](https://arxiv.org/abs/2503.15748).

[70] M. Horowitz, *1.1 computing’s energy problem (and what we can do about it)*, in *2014 IEEE International Solid-State Circuits Conference Digest of Technical Papers (ISSCC)*. 2014.

[71] C. Sun, T. K. Arrestad, V. Loncar, J. Ngadiuba, and M. Spiropulu, *Gradient-based Automatic Mixed Precision Quantization for Neural Networks On-Chip*, [arXiv:2405.00645 \[cs.LG\]](https://arxiv.org/abs/2405.00645).